# FACILE SYNTHESIS OF NICKEL MANGANESE SULFIDE ANCHORED GRAPHITIC CARBON NITRIDE/GRAPHENE ELECTRODE FOR SUPERCAPACITOR APPLICATION

Parthasarathi Bandyopadhyay[1], Thanh Tuan Nguyen[1], Dai Jiu Yi[1], Nam Hoon Kim[1*] and Joong Hee Lee[1,2*].

[1] Advanced Materials Institute of BIN Technology (BK21 plus Global) & Dept. of BIN Convergence Technology, Chonbuk National University, Jeonju, Jeonbuk 54896, Republic of Korea.

[2] Carbon Composite Research Centre, Department of Polymer & Nanoscience and Technology, Chonbuk National University Jeonju, Jeonbuk 54896, Republic of Korea. (*jhl@chonbuk.ac.kr and nhk@chonbuk.ac.kr)

**Keywords:** Graphene, Nickel nitrate hexahydrate, Supercapacitor, Specific capacitance.

## ABSTRACT

The nickel manganese sulfide (Ni-Mn-S) anchored on graphitic carbon nitride/graphene (g-$C_3N_4$-G) composite (Ni-Mn-S/g-$C_3N_4$-G) was prepared via a one-pot solvothermal method for supercapacitor application. FE-SEM and TEM analyses confirmed that the Ni-Mn-S nanoparticles were attached with the graphitic carbon nitride/graphene nanosheets (g-$C_3N_4$-G). The g-$C_3N_4$-G sheets deliver a large surface area to reduce self-aggregation and confine the morphology of the Ni-Mn-S particles, resulting highly conductive network of Ni-Mn-S/g-$C_3N_4$-G. Ni-Mn-S/g-$C_3N_4$-G based electrode exhibited high specific capacitance of 1697 F $g^{-1}$ at a current density of 1 A $g^{-1}$ and excellent rate capability (91% capacity retention after 2,000 cycles at 10 A $g^{-1}$) due to the abundant porous nanostructure, relatively high specific surface area, well-defined spherical morphology, and the synergetic effect of Ni-Mn-S and g-$C_3N_4$-G.

## 1 INTRODUCTION

The supercapacitors (SCs) have attracted tremendous attention in the fields of electric vehicles, railways, military devices, telecommunications, consumer electronics, and others due to their high power capability and long cycling life [1,2]. Extensive research has been carried out on transition metal oxides, hydroxides and sulfides as electrode materials for supercapacitors due to their pseudocapacitive properties and higher energy densities than those of carbon-based electrochemical double layer capacitors [1,3-5]. However, the low specific surface area, less interaction with the electrolyte, and low electrical conductivity limit the capacitive performance of transitional metal oxides, hydroxides and sulfides [1,6]. Therefore, various approaches have been taken to improve electrochemical performance of the transitional metal oxides, hydroxides, and sulfides as electrode materials for supercapacitor. Transition-metal sulfides are very promising candidates due to their excellent electrical conductivity and exceptional redox properties compared to transition metal oxides and hydroxides [7-9]. The ternary nickel manganese sulfide (Ni−Mn−S) can provide better electrochemical performance compared to the binary metal sulfides due to the combination of the strong redox properties of nickel and manganese ions in Ni−Mn−S. Ni−Mn−S can produce high electrical conductivity and high electrocatalytic activity due to the lower electronegative properties of sulfur. However, the Ni−Mn−S electrode can degrade into Ni and Mn ions and dissolve into electrolyte during the cycling performance. Besides, self-agglomeration of Ni−Mn−S material can decrease its electrochemical performance. Therefore, it is very important to design the structure and composition of the material for the fabrication of high-performance electrode material. In this context, graphene can serve as a perfect matrix material to uniformly disperse transitional metal sulfide materials due to unique structure, ultrahigh specific surface area, excellent mechanical strength and high electrical conductivity of graphene [8,10,11]. Recently, graphitic carbon nitride shows excellent potential for application in different energy conversion processes due to its high nitrogen content,

unique electronic structure and environmentally friendly natures [2]. However, low electronic conductivity and low specific surface area of graphitic carbon nitride (g-$C_3N_4$) limit its application in electrochemical-related applications. The g-$C_3N_4$ based graphene can increase the conductivity and electrocatalytic properties of g-$C_3N_4$ [2]. It is expected that g-$C_3N_4$ based graphene can be used as perfect matrix to prepare metal sulfide based electrode materials. Herein, we report a facile and cost-effective method to prepare Ni−Mn−S/g-$C_3N_4$-G through a one-step hydrothermal co-deposition method. It is expected that the combination of g-$C_3N_4$ and graphene can improve the interaction with the electrolyte and enable fast electron movement to accomplish a fast charge-discharge process for Ni-Mn-S/g-$C_3N_4$-G. The capacitive performance of the Ni-Mn-S/g-$C_3N_4$-G based electrode was evaluated by in a three electrode setup using 6 M KOH.

## 2 EXPERIMENTAL

### 2.1 Synthesis of the Ni-Mn-S/g-$C_3N_4$-G

Graphite oxide was synthesized from natural graphite powder through a modified Hummer's method [12]. Two-dimensional graphitic carbon nitride nanosheet was prepared according to the literature [13]. The Ni-Mn-S/g-$C_3N_4$-G composite was synthesized by a single-step solvothermal method. 50 mg of graphite oxide was mixed with 50 mL of DI water and dispersed using ultrasonic treatment for 1 h to convert graphite oxide into graphene oxide (GO). After that, 2.5 mg of g-$C_3N_4$ was added to the GO dispersion, and the mixture was subjected to ultrasonic for 1 h to form a uniform suspension. Then 0.35 mM of $Ni(NO_3)_2 \cdot 6H_2O$ and 0.60 mM of $Mn(NO_3)_2 \cdot 4H_2O$ were dissolved in 30 mL ethanol, and this metal solution was added to the g-$C_3N_4$/GO suspension, followed by sonication for 30 min to form a stable dispersion. The 5 mM of thiourea was added to the above dispersion and sonicated for 30 mints. Subsequently, the mixture was vigorously stirred for 6h at room temperature. Finally, the mixture was then transferred to a 100 mL Teflon-lined stainless steel autoclave, sealed tightly, and heated at 180 $^oC$ for 18 h. The resultant product was centrifuged and washed with water and ethanol several times. The obtained material was dried under vacuum oven at 80 °C for 12 h to remove the residual solvents.

### 2.2 Material characterization

The morphology of the and microstructure was investigated using field emission scanning electron microscopy (FE-SEM) and transmission electron microscopy (TEM). The FE-SEM images and energy dispersive X-ray analysis (EDAX) spectra were recorded by using a JSM-6701F instrument (JEOL Co., Japan) installed in the Center for University-Wide Research Facilities (CURF) at Chonbuk National University. The TEM images and energy dispersive X-ray spectroscopy (EDS) mapping were recorded using an H-7650 (Hitachi Ltd., Japan) in the Jeonju Center at KBSI.

### 2.3 Electrochemical measurements

The Ni-Mn-S/g-$C_3N_4$-G, carbon black and poly(vinylidene fluoride) mixed homogenously with a mass ratio of 8 : 1 : 1 in N-methyl-2-pyrrolidinone to make the slurry. The as-prepared slurry was coated on Ni foam (1 $cm^2$ in size), and then dried at 60 $^oC$ under vacuum. The slurry coated Ni foam was pressed for 60 s under 8.0 MPa. Then the Ni foam was used as the working electrode. The AgCl/Ag and Pt foil were used as the reference and the counter electrodes, respectively. Cyclic voltammetry (CV), galvanostatic charge-discharge (GCD), cyclic stability test and electrochemical impedance spectroscopy (EIS) measurements were performed using a potentiostat (CH660D, USA) electrochemicalwork station in a 6 M KOH electrolyte using a three electrode setup.

## 3. RESULTS AND DISCUSSION

### 3.1 FESEM analysis

The surface morphology of the Ni-Mn-S/g-$C_3N_4$-G composite was examined using FE-SEM analysis. The FE-SEM image illustrates that the Ni−Mn−S particles were uniformly distributed in the g-$C_3N_4$-G sheets (Figure 1a). The g-$C_3N_4$-G sheets can effectively preclude the self-aggregation of

Ni−Mn−S particles and avoid degradation during the galvanostatic charge–discharge cycle. Additionally, the synergistic interaction between Ni−Mn−S and the g-$C_3N_4$-G sheets can improve the electron transport properties for rapid transfer of the $K^+$ ion and electrons at the interfaces. The presence of elements such as Ni, Mn, S, carbon, and oxygen was evaluated by EDAX analysis, which is shown in Figure 1b.

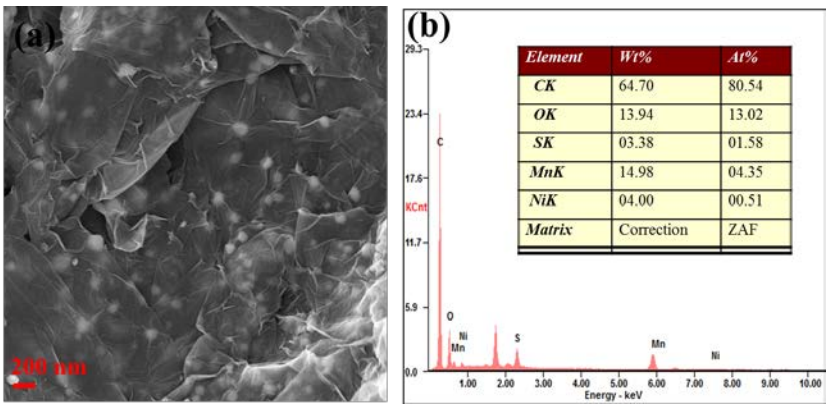


Figure 1: (a) FE-SEM image, and (b) EDAX spectrum of the Ni-Mn-S/g-$C_3N_4$-G composite.

### 3.2 TEM analysis

The morphology of the Ni-Mn-S/g-$C_3N_4$-G composite was determined using TEM analysis (Figure 2).

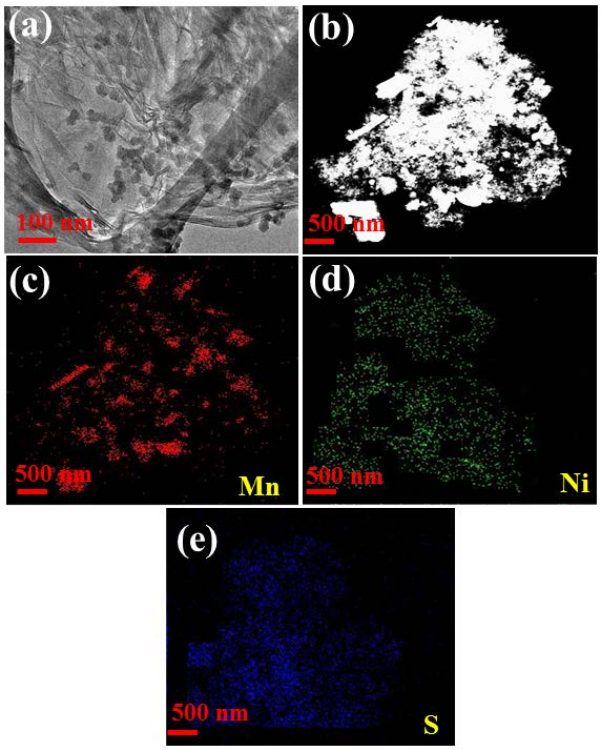


Figure 2: (a) TEM image of the Ni-Mn-S/g-$C_3N_4$-G composite and dark-field STEM elemental mapping of the Ni-Mn-S/g-$C_3N_4$-G composite: (b) selected area and elemental mapping of (c) Mn, (d) Ni, and (e) S.

The Ni−Mn−S particles were uniformly attached to the g-$C_3N_4$-G sheets in Ni-Mn-S/g-$C_3N_4$-G, as shown in Figure 2a. The elemental distribution and morphology of the Ni-Mn-S/g-$C_3N_4$-G composite were further examined by STEM with energy dispersive X-ray spectroscopy (EDS) analysis. Fig. 2b

shows the dark-field STEM images of Ni-Mn-S/g-$C_3N_4$-G. The EDS mapping shows that nickel, manganese, and sulfur were uniformly dispersed and also successfully anchored in the g-$C_3N_4$-G matrices (Figure 2c-2e). The detailed TEM analyses illustrate the formation of Ni-Mn-S/g-$C_3N_4$-G hybrid in which the active Ni−Mn−S particles with a uniform size are encapsulated by g-$C_3N_4$-G. TEM results also confirmed that there was no phase separation observed in Ni-Mn-S/g-$C_3N_4$-G at the nanometer scale during the preparation. The TEM analyses also confirmed the formation of Ni-Mn-S/g-$C_3N_4$-G composite in which Ni−Mn−S particles were uniformly decorated on the g-$C_3N_4$-G sheet.

### 3.3 Supercapacitors performance

Figure 3a shows the cyclic voltammetry (CV) curve of the Ni-Mn-S/g-$C_3N_4$-G based electrode material at different scan rates (10-150 mV) in a 6 M KOH aqueous electrolyte. The CV curves show a pair of well-defined redox peaks, confirming that the capacitance property is complemented by faradic redox reactions [1,4]. The area under the CV curve increased and remained steady with the increase of scan rate for Ni-Mn-S/g-$C_3N_4$-G, suggesting the rates of electronic and ionic movement are sufficiently fast at the different potentials. Figure 3b displays the galvanostatic charge-discharge (CD) curves of the Ni-Mn-S/g-$C_3N_4$-G based electrode at different current densities ranging from 1-10 A $g^{-1}$. The specific capacitance (*C*) values of all materials were determined from the CD curve according to the following equation [3-5]:

$$C = \frac{\Delta t \times I}{\Delta V \times m}$$

where, $\Delta t$ is the discharge time, I is the discharge current, $\Delta V$ is the working potential window during discharge, and m is deposited mass on the Ni-foam. The Ni-Mn-S/g-$C_3N_4$-G based electrode exhibited an excellent *C* of 1697 F $g^{-1}$ at a current density of 1 A $g^{-1}$. The C values were calculated to be of 1697, 1372, 1021, and 562 at current densities of 1, 3, 5, and 8 A $g^{-1}$, respectively. The *C* values decreased with the increase in current density due to the ascending voltage drop. The Ni-Mn-S/g-$C_3N_4$-G composite shows a higher specific capacitance due to the strong attachment between the Ni-Mn-S and g-$C_3N_4$-G sheets. Besides, the synergistic interaction between Ni and Mn ions in the Ni-Mn-S/g-$C_3N_4$-G composite increased the pseudocapacitive properties of the electrode, resulting in a higher specific capacitance value [1,3]. The intercalation of graphene sheets enhances the electron transport property of Ni-Mn-S, thereby improves the synergistic effect of Ni-Mn-S/g-$C_3N_4$-G. Figure 3c shows the Nyquist plots of the Ni-Mn-S/g-$C_3N_4$-G. The Nyquist plot involves a quasi-semicircle in the high-frequency region and a straight line in the low-frequency region, signifying ideal capacitive behavior of the Ni-Mn-S/g-$C_3N_4$-G. The first intersection point of the curve on the Z′ axis signifies series resistance (Rs) and Rs value was found to be of 0.83 Ω. It indicates high conductivity of the electrodes and the low contact resistance between the active material/current collector. The cyclic stability plot of the Ni-Mn-S/g-$C_3N_4$-G composite is shown in Figure 3d. Ni-Mn-S/g-$C_3N_4$-G maintained 92 % of its original specific capacitance at a high current density of 10 A $g^{-1}$ in 6 M KOH solution after 2000 charge−discharge cycles. These results demonstrated the Ni-Mn-S/g-$C_3N_4$-G composite as an ultra-durable electrode material for supercapacitor application. The interfacial area between Ni-Mn-S and electrolyte increases with the increase in the reaction time, resulting good electrochemical stability of the Ni-Mn-S/g-$C_3N_4$-G. Therefore, the higher capacitive performance of Ni-Mn-S/g-$C_3N_4$-G electrode material is due to the (i) Ni-Mn-S particles and g-$C_3N_4$-G sheets make Ni-Mn-S/g-$C_3N_4$-G composite as highly conductive electron transport medium. (ii) intercalation of graphene sheets, and (iii) uniform distribution of the Ni-Mn-S nanoparticle with improved synergistic effect [7,9].

## 4. CONCLUSIONS

In this work, novel Ni-Mn-S/g-$C_3N_4$-G hybrid was successfully fabricated using a one-step hydrothermal co-deposition method. In the composite architecture, Ni-Mn-S particles are well distributed on the flexible g-$C_3N_4$-G nanosheets as confirmed from the FESEM and TEM analyses. Ni-Mn-S/g-$C_3N_4$-G based electrode produced a maximum specific capacitance of 1697 F $g^{-1}$ at 1 A $g^{-1}$ in 6 M KOH aqueous electrolyte. The high specific surface area and well-defined spherical morphology

improve the interaction with the electrolyte and promote fast ion diffusion, resulting higher capacitance value. Ni-Mn-S/g-$C_3N_4$-G showed excellent rate capability due to the synergetic interaction between from the Ni-Mn-S and g-$C_3N_4$-G. The electrode also exhibited good cycling stability and maintained 92% of its original capacitance after 2,000 cycles. Therefore, as-synthesized the Ni-Mn-S/g-$C_3N_4$-G composite can be utilized as a high performance electrode material for supercapacitor due to its higher specific capacitance and outstanding stability.

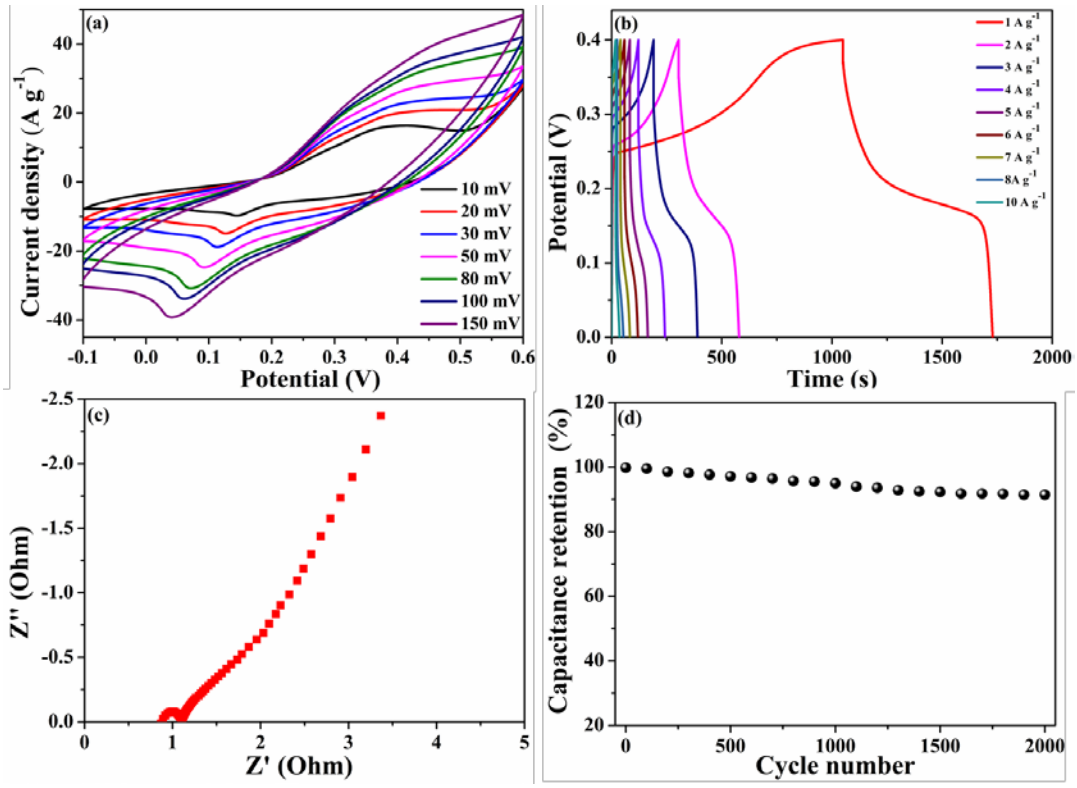


Figure 3: (a) CV curves at different scan rates, (b) galvanostatic charge–discharge curves at different current densities, (c) Nyquist plots, and (d) cyclic stabilities at 10 A $g^{-1}$ for 2000 cycles of Ni-Mn-S/g-$C_3N_4$-G composite.

## ACKNOWLEDGEMENTS

This research was supported by the Basic Research Laboratory Program (2014R1A4A1008140), Nano-Material Technology Development Program (2016M3A7B4900117), and Basic Science Research Program (2017R1A2B3004917) through the National Research Foundation (NRF) funded by the Ministry of Science, ICT & Future Planning of Republic of Korea.

## REFERENCES

[1] H. Chen, S. Zhou, and L. Wu, Porous nickel hydroxide-manganese dioxide-reduced graphene oxide ternary hybrid spheres as excellent supercapacitor electrode materials, *ACS Applied Material Interfaces*, **6**, 2014, pp. 8621−8630 (doi: 10.1021/am5014375).

[2] Q. Chen, Y. Zhao, X. Huang, N. Chen and L. Qu, Three-dimensional graphitic carbon nitride functionalized graphene-based high-performance supercapacitors, *Journal of Materials Chemistry A*, **3**, 2015, pp. 6761–6766 (doi: 10.1039/c5ta00734h).

[3] J. Zhao, J. Chen, S. Xu, M. Shao, Q. Zhang , F. Wei, J. Ma, Mi. Wei, D.G. Evans and X. Duan, Hierarchical NiMn layered double hydroxide/carbon nanotubes architecture with superb energy

density for flexible supercapacitors, *Advanced Functional Material*, **24**, 2014, pp. 2938–2946 (doi: 10.1002/adfm.201303638).

[4] P. Hao, J. Tian, Y.H. Sang, C.C. Tuan, G.W. Cui, X.F. Shi, C.P. Wong, B. Tang and H. Liu, 1D Ni–Co oxide and sulfide nanoarray/carbon aerogel hybrid nanostructures for asymmetric supercapacitors with high energy density and excellent cycling stability, *Nanoscale*, **8**, 2016, pp. 16292–16301 (doi: 10.1039/C6NR05385H).

[5] L.J. Xie, J.F. Wu, C.M. Chen, C.M. Zhang, L. Wan, J.L. Wang, Q.Q. Kong, C.X. Lv, K.X. Li and G.H. Sun, A novel asymmetric supercapacitor with an activated carbon cathode and a reduced graphene oxide-cobalt oxide nanocomposite anode, *Journal of Power Sources*, **242**, 2013, pp. 148–156 (doi: 10.1016/j.jpowsour.2013.05.081).

[6] H. Wang, H. Yi, X. Chen and X. Wang, Asymmetric supercapacitors based on nanoarchitectured nickel oxide/graphene foam and hierarchical porous nitrogen-doped carbon nanotubes with ultrahigh-rate performance, *Journal of Materials Chemistry A*, **2**, 2014, pp. 3223–3230 (doi: 10.1039/c3ta15046a).

[7] M. Shen, C. Ruan, Y. Chen, C. Jiang, K. Ai and L. Lu, Covalent entrapment of cobalt–iron sulfides in n-doped mesoporous carbon: extraordinary bifunctional electrocatalysts for oxygen reduction and evolution reactions, *ACS Applied Material Interfaces*, **7**, 2015, pp. 1207–1218 (doi: 10.1021/am507033x).

[8] X. Cao, Z. Yin and H. Zhang, Three-dimensional graphene materials: preparation, structures and application in supercapacitors, *Energy & Environmental Science*, **7**, 2014, pp. 1850–1865 (doi: 10.1039/c4ee00050a).

[9] S. Peng, L. Li, C. Li, H. Tan, R. Cai, H. Yu, S. Mhaisalkar, M. Srinivasan, S. Ramakrishna and Q. Yan, *In situ* growth of $NiCo_2S_4$ nanosheets on graphene for high-performance supercapacitors, *Chemical Communications*, **49**, 2013, pp. 10178–10180 (doi: 10.1039/C3CC46034G).

[10] J. Duan, S. Chen, M. Jaroniec and S.Z. Qiao, Heteroatom-Doped Graphene-Based Materials for Energy-Relevant Electrocatalytic Processes, *ACS Catalysis*, **5**, 2015, pp. 5207–5234 (doi: 10.1021/acscatal.5b00991).

[11] W. Yang, Z. Gao, J. Wang, J. Ma, M. Zhang and L. Liu, Solvothermal one-step synthesis of Ni-Al layered double hydroxide/carbon nanotube/reduced graphene oxide sheet ternary nanocomposite with ultrahigh capacitance for supercapacitors, *ACS Applied Material Interfaces*, **5**, 2013, pp. 5443–5454 (doi: 10.1021/am4003843).

[12] W. Hummers and R. Offeman, Preparation of graphitic oxide**,** *Journal of American Chemical Society*, **80**, 1958, pp. 1339-1339 (doi: 10.1021/ja01539a017).

[13] T.Y. Ma, Y. Tang, S. Dai and S.Z. Qiao, Proton-functionalized two-dimensional graphitic carbon nitride nanosheet: an excellent metal-/label-free biosensing platform, *Small*, 10, 2014, pp. 2382–2389 (doi: 10.1002/smll.201303827).